Analysis of radial-outflow turbine design for supercritical CO2 and comparison to radial-inflow turbines

Grönman Aki, Uusitalo Antti

DOI: 10.1016/j.enconman.2021.115089

Energy Conversion and Management 252 (2022) 115089

Contents lists available at ScienceDirect

Energy Conversion and Management

journal homepage: www.elsevier.com/locate/enconman

Analysis of radial-outflow turbine design for supercritical CO_2 and comparison to radial-inflow turbines

Aki Grönman *, Antti Uusitalo

LUT University, School of Energy Systems, Yliopistonkatu 34, P.O. Box 20, 53851 Lappeenranta, Finland

ARTICLE INFO

Keywords:
Radial outflow turbine
Radial inflow turbine
Supercritical CO_2 power cycle
Recompression cycle
Turbomachinery loss

ABSTRACT

Cycles using supercritical carbon dioxide have been recognized as potential future power technology. However, the turbines in these systems tend to experience very high rotational speeds and entail small physical sizes, which can affect on the overall feasibility. One turbine type having potential to overcome some of the described challenges is the radial outflow turbine. However, its use in supercritical carbon dioxide power systems has not yet been extensively studied since typically axial or radial inflow turbines are considered instead. In this paper, the design of radial-outflow turbines with supercritical carbon dioxide is carried out and the results are compared to the respective radial inflow turbine designs. The analysis was carried out with turbine inlet temperature of 600 °C, inlet pressure of 200 bar and outlet pressure of 78 bar. Designs with four mass flow rates were investigated to study the effect of the power scale on the turbine design and losses. The geometry, efficiency, rotor stress and axial force were defined and analyzed for each design case. The results show that both the investigated turbine types can reach high isentropic efficiencies ranging from about 85% to over 90%. The radial outflow turbines can reach high efficiencies at wider specific speed range whereas the efficiency of radial inflow turbine is reduced more steeply, as the design speed is changed from its optimal value. Radial outflow turbines also reach high efficiencies with lower design speeds and that can be considered advantageous, since it helps to reduce the challenges related to turbomachinery rotordynamic and mechanical design. As a conclusion of the study, it is suggested that the use of radial outflow turbines can increase the feasibility of supercritical carbon dioxide power systems at the examined power scales.

1. Introduction

The use of supercritical carbon dioxide (SCO_2) as a working fluid has been identified as a promising power generation technology candidate for producing electricity with reduced environmental impacts, a small plant foot print, and high conversion efficiency [1]. They have been suggested for various applications, including future nuclear reactors [2], waste heat recovery [3,4], and concentrating solar power [5,6]. In addition, this technology could replace the use of steam turbine cycles in large-scale power plants [7]. Combining the supercritical CO_2 power cycle with oxy-combustion could further lead to realizing power technologies with the capability to utilize fossil fuels at a high conversion efficiency, together with full carbon capture in the future [8]. Various cycle layouts, including different numbers and placements of turbomachines and heat exchangers have been proposed and investigated intensively to maximize the power output of SCO_2 cycles for different power scales and temperatures [7]. A recompression cycle layout with two compressors, one turbine as well as high-temperature and low temperature recuperators, has been identified as one of the most promising cycle layout options, especially for high temperature SCO_2 power plants [9,10].

In a recent study by Romei et al. [11], it was observed that the efficiency of the whole SCO_2 power cycle is highly affected by the efficiency and operation of turbines and the compressors of the cycle [11]. Thus, the design of turbomachines capable of achieving high-efficiency operation is one of the key issues in reaching the full potential of SCO_2 power technology in the future. In previous studies by Li et al. [12] and Sarkar [10] it was revealed that the power output of the recompression CO_2 cycle is more sensitive to the turbine efficiency when compared to a respective change in the compressor efficiency. Thus, it is highly important that especially the turbines of SCO_2 cycles can be operated at high efficiencies. Different types of turbomachines have been considered and designed for SCO_2 power plants. In the majority of the recent studies, either axial flow turbines (e.g., [13,14]) or radial inflow turbines (e.g., [15–17]) have been considered as suitable turbine types for

* Corresponding author.
E-mail address: aki.gronman@lut.fi (A. Grönman).

https://doi.org/10.1016/j.enconman.2021.115089
Received 30 September 2021; Received in revised form 9 November 2021; Accepted 29 November 2021

Nomenclature

Latin alphabet

b	blade height, m
b/c_x	aspect ratio, –
C	absolute velocity, m/s
c	chord/length to relative angle ratio, m
D	diameter, m
F	force, N
f	friction factor, –
h	specific enthalpy, kJ/kg
K_p	rotor loss coefficient, –
L	length, m
n	rotational speed, rpm
N_s	Specific speed, –
P	power, W
p	pressure, bar
q_m	mass flow rate, kg/s
q_v	volumetric flow rate, m^3/s
R	radius, m
R	degree of reaction, –
Re	Reynolds number, –
T	temperature, °C
t_c	clearance height, m
U	peripheral velocity, m/s
W	relative velocity, m/s
Z	number of blades, –
x	blade thickness, m

Greek alphabet

α	angle of absolute velocity, °
β	angle of relative velocity, °
ϵ	stator or rotor deflection, °
ζ	stator or rotor loss coefficient, –
η	efficiency, –
μ	viscosity, μPas
ξ	stator pressure ratio factor, turning loss coefficient, –
ρ	density, kg/m^3
σ	stress, MPa
ω	angular speed, rad/s

Subscripts

df	disk friction
inc	incidence
ex	exit
h	hydraulic
hub	blade or vane hub
hyd	hydraulic
i	incidence
m	meanline
max	maximum
nozzle	nozzle
opt	optimal
vpass	passage
r	radial component
rot	rotor
s	isentropic
sh	shroud
shaft	shaft
stat	stator
tip	blade tip/shroud
tc	tip clearance
u	tangential component
1	stator inlet, impeller outlet, impeller inlet
2	rotor inlet/stator outlet, impeller outlet, impeller inlet
3	rotor outlet

Abbreviations

CFD	Computational fluid dynamics
RIT	Radial–inflow turbine
ROT	Radial-outflow turbine
SCO_2	Supercritical carbon dioxide

SCO_2 power cycles. One of the main factors defining the most suitable turbine type is the power scale as it has a high impact on the turbine geometry, required rotational speed and losses. In general, axial turbines have been more often considered as suitable for higher power applications whereas radial turbomachines have been considered as more suitable for smaller-scale systems [19]. Based on a rough technological categorization of SCO_2 systems, axial turbines have been evaluated as more suitable for power levels above 10 MW and radial inflow turbines for power outputs below this limit [19]. However, as the use of SCO_2 leads to small scale turbomachines with high rotational speeds, radial inflow turbines (RIT) have been identified to be able to reach high efficiencies even at 20 MW [17] to 30 MW [18] power scales. One turbine type that has been recently studied for different applications, but not widely considered for SCO_2, is the radial outflow turbine (ROT). This turbine type has similar features to both axial and radial inflow machines and it has been suggested to provide high efficiency designs especially for low specific speeds [20]. Thus, the radial outflow turbine may have a good potential to help reduce the otherwise reasonably high rotational speeds and yet maintain high efficiency. The use of radial outflow turbines have been recently considered for ORC-applications [21–23], for steam Rankine cycles [20], and very limitedly also for supercritical CO_2 [24].

In general, it has been reported that significantly high turbine isentropic efficiencies ranging from about 80 % to over 90 % can be reached for SCO_2 turbines even at rather low power levels. Radial inflow turbines have been investigated for SCO_2 power plants recently. Lv et al. [15] studied the aerodynamic design and losses of radial-inflow turbines operating with supercritical CO_2. Their analysis showed that the radial-inflow turbines can achieve high efficiencies and they observed that the main loss sources were the stator loss, rotor loss, clearance loss and exit kinetic loss. Unglaube and Chiang [16] investigated the design of SCO_2 driven radial-inflow turbines and suggested optimal specific speed range of 0.2 to 0.5 for the turbine design, as they observed additional losses caused by higher velocities with high specific speed turbine designs. Lee and Gurgenci [17] studied the design and losses of SCO_2 driven radial-inflow turbines with three different design methods and with four different power levels of 300 kW, 1 MW, 10 MW, and 20 MW. The investigated methods included the Aungier's, Moustapha's and Whitfield and Baines' method. They observed that the Aungier's and Moustapha's methods resulted in almost similar designs and efficiencies, whereas the Whitfied and Baines' method predicted slightly higher losses when compared to the other approaches. Uusitalo et al. [25] studied the design of supercritical CO_2 radial inflow turbines with the design power ranging from a few hundred kW to 3.5 MW. The power scale was observed to have a high effect on the turbine efficiency, as especially the tip clearance loss significantly increased for low power level turbine designs. It was concluded that the efficiency of SCO_2 radial inflow turbines with different specific speeds follow the efficiency graphs well by Balje [26] and Rohlik [27,28], that are based on turbine designs with ideal gas flows.

Recently, the use of radial outflow turbines has been also investigated for SCO_2 by Luo et al. [24]. The investigated turbine had a power

output of 10 MW and it consisted of a single turbine stage. A high total-to-static efficiency of 89.02% was achieved in their study for an optimized SCO_2 radial outflow turbine. Other studies investigating the use and design of ROTs with different real gases can also be found in the literature. Recently, Kim and Kim [23] studied the design of a ROT for a 400 kW application using R134a as the working fluid, whereas smaller-scale ROT designs have also been considered previously for ORC system with different non-conventional fluids [21,22].

In addition to the small physical sizes and high rotational speeds of the SCO_2 turbines, also the axial force has an important role regarding the feasibility of the power cycle. Ma et al. [29] highlighted that despite the small physical size of the turbomachines, the axial force caused by SCO_2 turbines is significantly higher when compared to the design of typical steam and gas turbines, which makes the estimation of axial force an important parameter to be considered. They suggested that the axial force can be lowered and the difficulties in designing the axial bearing can be avoided by using an impeller back disk design with radial pump-out vanes. The same method is widely used in the pump industry to reduce the axial force of centrifugal pump impellers and could be exploited in SCO_2 turbine technology.

The literature review shows that there is some research work already done related to the design, operation and losses of supercritical CO_2 driven turbines, especially with axial and radial inflow turbines. However, the information on how the design-specific speed and power level affect the turbine design and losses is scarce in the literature, especially when different turbine types are considered and compared. In addition, the radial outflow turbines have been recently identified as a potential turbine type for many power applications, but currently there are only a few studies considering the use of this turbine type for supercritical fluids. In this study, the design of ROTs operating with supercritical CO_2 was investigated with different design powers and with different specific speeds. The ROT designs and losses were compared against respective RIT designs, which is the turbine type often considered for small-scale SCO_2 power systems. The specific focus, novelty and the original contribution of the study are to investigate the geometry, rotational speed, optimal specific speed range and loss distribution with the two different turbine types to increase understanding on the selection of the suitable turbine type for small-scale and high-temperature SCO_2 power systems, and especially, to evaluate the feasibility of radial outflow turbine technology for SCO_2 power systems. In addition, an axial force analysis and preliminary impeller strength analysis for the different designs are included to study the differences between the two turbine types also from the mechanical design point of view. Based on the designs, the different turbine types are compared and their pros and cons are discussed and highlighted. In comparison with the previous studies by the authors, the current study extends the validity of the radial outflow turbine design approach presented by Grönman et al. [20] from steam turbines also for supercritical CO_2 applications. Compared with the previous RIT studies by the authors [25,37], the current study uses the loss prediction methodology presented for RITs in [25], which was numerically verified in [37], as a comparison data for the ROTs.

The article begins with the presentation of the modeling methods used in the analysis of both turbine types and includes the verification of turbine design approaches. This section is followed by the comparison of general performance and geometrical parameters before the detailed loss analysis. Prior to concluding the work in its own section, both axial force and impeller stress analyses are conducted.

2. Methods

The methods used for the design and loss analysis of the turbines are presented in the following. First, the methods used in the radial outflow turbine design and the developed 1D code are presented in detail. Second, the design methods used for the radial-inflow turbines are shortly presented and summarized. The code verifications are shown in the third sub-section, which is followed by a presentation of the axial force estimation and impeller stress modeling approaches. In comparison with the chosen 1D design approach, the 2D and 3D approaches offer the benefit of a more detailed insight on the flow phenomena. However, a lower computational requirement and less complex design code favor the 1D approach.

The turbine inlet conditions of 200 bar and 600 °C were selected for the analysis for all the turbine design cases. Turbine inlet values close to the selected ones have been considered suitable in many thermodynamic analysis studies concerning recompression cycles and other high temperature SCO_2 cycles (e.g. [9,10]). A turbine outlet pressure of 78 bar was used in order to maintain the turbine outlet at a supercritical fluid state. Both turbine types were designed with four different mass flow rates of 5 kg/s, 10 kg/s, 20 kg/s and 40 kg/s, in order to investigate the effect of turbine design power scale on the geometry and losses. The radial inflow turbines were designed for an N_s range of 0.35 to 0.7 that was estimated as the most feasible range for this turbine type [28]. The radial outflow turbine designs were investigated with the specific speed range of 0.1 to 0.7.

2.1. Radial-outflow turbine geometry and losses

The radial outflow turbine design process follows main principles which are similar to those applicable to axial turbines. Two of the biggest differences are that the radial velocity is used instead of the axial velocity and that the pitch-to-chord ratio varies between the inlet and outlet of each blade row. In pitch-to-chord ratio the pitch is defined as a circumferential distance between two vanes or blades either at the leading or the trailing edge. As a result of the design, vane and blade dimensions, velocity triangles, and performance parameters are obtained. Detailed descriptions of the general design principles are presented in Grönman et al. [20] and by Grönman et al. [38]. In this work, only single-stage single-flow turbines were studied, since a preliminary assessment suggested that multi-stage or double-flow machines may easily lead to unfeasible blade heights (below 2 mm). Examples of the radial outflow turbine geometry and a typical rotor inlet velocity triangle are illustrated in Fig. 1 (a) and (b).

In the design process, the fluid mass flow, turbine rotational speed, static inlet and outlet pressures, and static inlet temperature are given as input values. The Refprop database was used to provide fluid properties [39]. The calculation is based on iterating the turbine efficiency, rotor inlet radius, and radial velocities. The rotor inlet radius and radial velocity are used to control both the blade height and the end wall opening angle. Traupel's method [40] is used to solve the optimal pitch-to-chord ratios. For all input values, the aim is to find a geometry that fulfills the following design criteria:

- The blade row radial clearance must be 30% of the vane radial chord.
- The end wall opening angle (the blade passage height increase angle in the radial direction) must be less than 30 degrees following Persico et al. [41].
- The degree of reaction should be 0.5.

The calculation of turbine losses was based on Soderberg's method [42], which was developed during a time when low aspect ratios were commonly used. The performance of Soderbergs' turbine loss models with ultra low aspect ratio (aspect ratio less than unity) radial outflow turbines has been verified in two previous studies by Grönman et al. [20] and by Grönman et al. [38]. According to a study by Zhdanov et al. [43], the used method was able to predict the turbine efficiency with an accuracy of ±3%. In the loss model, the stator loss is defined as

$$\zeta_{stat} = \left(\frac{10^5}{Re}\right)^{1/4}\left[\left(1+\xi\right)\left(0.993+0.021\frac{c_r}{b}\right)-1\right], \quad (1)$$

and rotor loss as

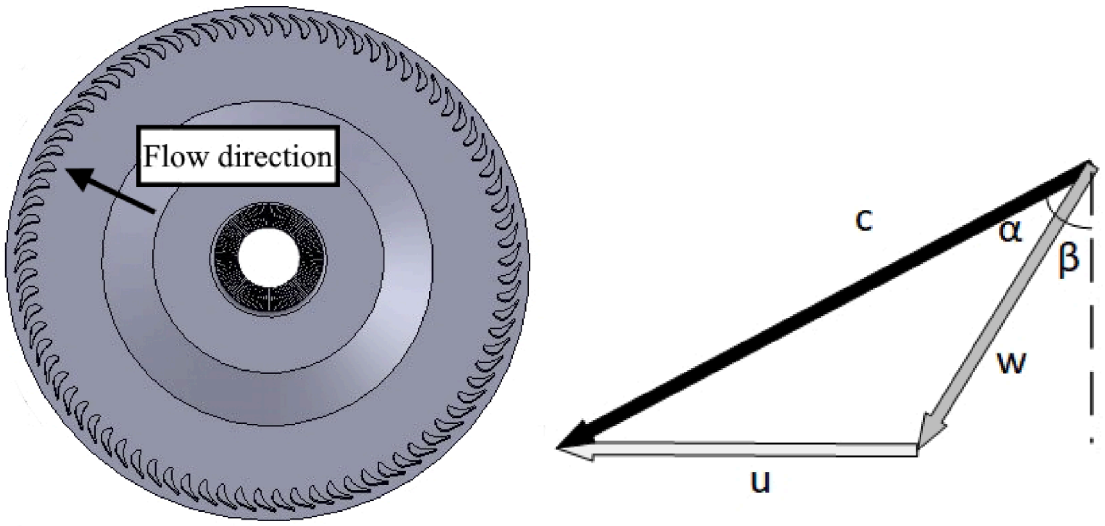

Fig. 1. Example of a single-stage radial outflow turbine rotor geometry (a) and typical rotor inlet velocity triangle for a radial outflow turbine (b).

$$\zeta_{rot} = \left(\frac{10^5}{Re}\right)^{1/4}\left[\left(1+\xi\right)\left(0.975+0.075\frac{c_r}{b}\right)-1\right]. \quad (2)$$

In Eqs. 1 and 2 the turning loss ξ is expressed as a function of deflection ϵ

$$\xi = 0.04 + 0.06\left(\frac{\epsilon}{100}\right)^2. \quad (3)$$

The loss model does not consider the effect of the tip-clearance on the turbine performance. Therefore, the tip-clearance loss is calculated following the recommendation by Dixon [42]. In that approach, the stage efficiency is multiplied by the ratio between the blade area and the total area including the tip-clearance to take those effects into account. The total-to-static isentropic efficiency is defined as

$$\eta_s = \left[1+\frac{\zeta_{rot}W_3^2+\zeta_{stat}C_2^2+C_1^2}{2(h_1-h_3)}\right]^{-1}. \quad (4)$$

2.2. Radial-inflow turbine geometry and losses

Radial inflow turbine geometries and losses were estimated using the design and loss analysis methods presented in detail in [25]. The mass flow rate, turbine inlet conditions, outlet static pressure and initial guess for the turbine efficiency were given as the inputs for the calculation. The methods for solving the turbine geometry with the different design values were mainly based on the design principles and guidelines presented by Rohlik [28] and Balje [26]. The stator geometry and the rotor geometry were defined based on the given inputs. The geometry definition and loss calculations were based on solving the velocity triangles and the flow continuity equation at the stator outlet/rotor inlet and at the rotor outlet, as well as by using the Euler turbomachinery equation for connecting the enthalpy drop over the turbine and the velocities. Similar to the ROT designs, Refprop [39] was used to define the thermodynamic properties of the fluid at different parts of the turbine. An example of a radial-inflow turbine stator and rotor geometry and typical velocity triangle are presented in Figs. 2a and 2b.

Once the geometry of the turbine was solved, the different turbine losses were evaluated by using a set of existing enthalpy loss correlations for radial inflow turbines. The losses that were taken into account were the stator loss, rotor passage loss, tip clearance loss, incidence loss, disk friction loss, and the exit kinetic loss. The formulas of the implemented loss models and the corresponding literature references for each model are summarized in Table 1. Turbine loss predictions based on the selected set of loss correlations and the results of CFD-analysis for RIT design with different N_s were compared in [37] showing a relatively good agreement in the efficiency predictions between the two methods. The turbine total-to-static isentropic efficiency was defined as,

$$\eta_s = \frac{\Delta h_s - \Sigma\Delta h_{loss}}{\Delta h_s} \quad (5)$$

in where,

$$\Sigma\Delta h_{loss} = \Delta h_{stat} + \Delta h_{inc} + \Delta h_{tc} + \Delta h_{pass} + \Delta h_{df} + \Delta h_{ex}. \quad (6)$$

As the turbine efficiency has an influence on the turbine geometry definition, the solved efficiency was used as a new input for defining the updated geometry. The RIT design calculation was iterated until no significant changes in the turbine geometry or in the predicted losses

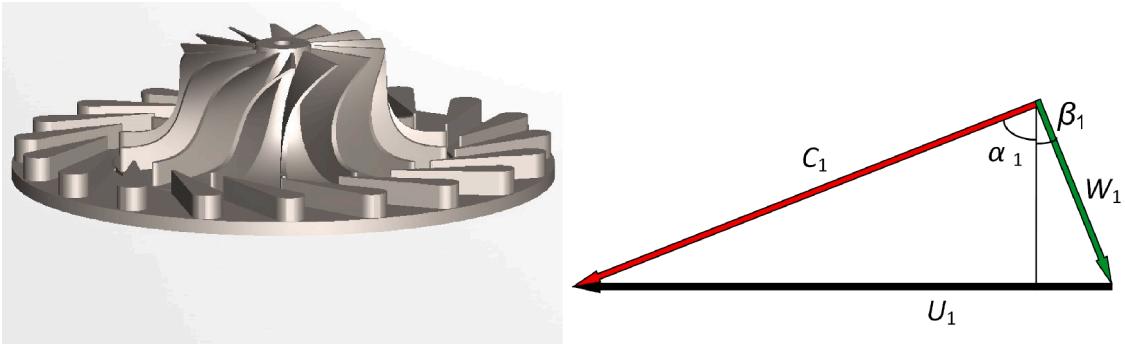

Fig. 2. Example of a radial turbine stator and rotor (a) and a typical rotor inlet velocity triangle for the radial inflow turbine (b).

Table 1
Loss correlations for radial-inflow turbine.

Loss	Loss correlation	Literature reference
Stator	$\Delta h_{stat}=4f_{nozzle}\overline{C}^2\frac{L_{hyd,nozzle}}{D_{hyd,nozzle}}$	Whitfield and Baines [30]
Incidence	$\Delta h_{inc}=\frac{W_{u1}^2}{2}$	Whitfield and Wallace [31]
Passage	$\Delta h_{pass}=K_p\left(\frac{L_h}{D_h}+0.684\left[1-\frac{R_{2m}}{R_1}\right]\frac{cos\beta_{2m}}{b_2/c}\right)0.5\left(W_1^2+W_2^2\right)$	NASA model [32]
Tip clearance	$\Delta h_{tc}=0.64\frac{t_c}{b_1}\sqrt{\frac{4\pi}{b_1Z}C_{u1}^3C_{r2}\frac{R_{2,tip}^2-R_{2,hub}^2}{\left(R_1-R_{2,tip}\right)\left(1+\frac{\rho_1}{\rho_2}\right)}}$	Jansen [33]
Disk friction	$\Delta h_{df}=0.5f\left(\rho_1+\rho_2\right)D_1^2\frac{U_1^3}{16q_m}$	Daily and Nece [34]
Exit kinetic loss	$\Delta h_{ex}=\frac{1}{2}c_2^2$	Lv et al. [15], Zhou et al. [35], and Rahbar et al.[36]

between the iteration rounds were observed.

2.3. Verification of the codes

The used turbine design codes were compared against the data available in the literature for supercritical CO_2 driven radial inflow turbines and a radial outflow turbine. In this work, the developed ROT design code was verified by using the 10 MW scale SCO_2 driven turbine by Luo et al. [24]. As seen in Table 2, the design code is able to reproduce the performance parameters well. For example, the turbine efficiency prediction is within the accuracy of the used loss model (±3% according to Zhdanov et al. [43]), when compared to both 1D and 3D results. The deviation in static pressure prediction is less than 0.5% and both the turbine power and the degree of reaction are also well predicted. All in all, the verification made gives a good foundation for further studies.

The RIT design code was verified against four different turbine designs [44,15,35] and the detailed verification study is presented in [25]. The results are reproduced here for the readers' convenience in Table 3. The comparison showed only minor deviations between the results of the design code and the turbine designs reported in the literature.

Table 2
Radial outflow turbine design code verification for supercritical CO_2.

Input	Luo et al. [24]	ROT design code	
q_m [kg/s]	164.6	164.6	
n [rpm]	6000	6000	
T_1 [K]	773	773	
p_1 [bar]	130.0	130.0	
p_3 [bar]	80.0	80.0	
D_1 [mm]	626.3	626.3	
Output			**Dev. [%]**
p_2 [bar]	96.2	96.6	0.4
R [-]	0.37	0.33	10.8
P [MW]	10.0	10.4	3.8
η_s (1D) [%]	88.7	90.7	2.2
η_s (CFD) [%]	89.0	-	-
α_2 [°]	78.0	78.4	0.5
β_2 [°]	44.0	51.0	13.7
β_3 [°]	75.3	75.1	0.3
D_3 [mm]	757.5	762.3	0.6
b [mm]	18.5	18.5	0

Deviations ranging from 0.3% to 6.9% in the turbine radii were observed and maximum deviations of below 13.3% were observed in the rotor blade heights. A maximum deviation of below 5% was observed between the predicted turbine efficiencies and the efficiencies reported in the literature. In addition, the efficiency prediction based on the selected set of loss correlations and results of a RANS CFD analysis using the k-ω SST model showed a relatively good agreement in the recent study [37] for RIT designs with different specific speeds with a mass flow rate of 9 kg/s.

2.4. Axial force estimation

The method for defining the axial force is presented in the following. In general, the higher the axial force caused by the turbine wheel, the more challenging it is to design the turbogenerator thrust bearings. In some cases, even a balance piston is required to compensate for the force. It has been observed that despite the small size of the SCO_2 turbomachines, the axial force caused by the impeller is higher than in typical steam and gas turbines, which makes the axial force analysis an important step in the design of SCO_2 turbines [29]. The high axial force can lead to high power losses in the turbogenerator, especially if force-balancing system is required. Thus, the axial force prediction of the different turbine designs was included in the analysis. The force was calculated by using a model by Nguen-Schäfer [45] that is capable of estimating the axial force for different types of centrifugal impellers. The results of this method were also compared against measurements recently by Tianen et al. [46] showing a relatively good agreement between the experimental results and the model. The axial force is composed of the turbine outlet force, shroud force, impulse force and the impeller back disk force.

$$F=F_{outlet}+F_{shroud}+F_{impulse}-F_{backdisk} \tag{7}$$

The equations for calculating the different forces are presented in the following:

$$F_{outlet}=p_2\frac{\pi}{4}D_{2sh}^2 \tag{8}$$

$$F_{shroud}=\frac{p_1+p_2}{2}\frac{\pi}{4}\left(D_1^2-D_{2sh}^2\right) \tag{9}$$

$$F_{impulse}=\frac{q_m^2R_{CO2}T_2}{p_2\frac{\pi}{4}\left(D_{2sh}^2-D_{2hub}^2\right)} \tag{10}$$

Table 3
Radial inflow turbine design code verification for supercritical CO2. The modeling results are reproduced from Uusitalo et al. [25].

Input	Qi et al. [44]	RIT design code		Qi et al. [44]	RIT design code	
q_m [kg/s]	1.04	1.04		2.08	2.08	
T_1 [°C]	560.0	560.0		560.0	560.0	
p_1 [bar]	200.0	200.0		200.0	200.0	
p_3 [bar]	90.09	90.09		90.09	90.09	
n, [krpm]	160.0	160.0		113.0	113.0	
Z [–]	9.0	9.0		9.0	9.0	
t_c, [mm]	0.1	0.1		0.1	0.1	
α_2, [deg]	72.0	72.0		72.0	72.0	
Output			Dev. [%]			Dev. [%]
R_2 [mm]	20.3	18.9	6.9	28.7	26.9	6.3
$R_{3,tip}$ [mm]	10.5	9.8	6.7	14.4	13.5	6.3
$R_{3,hub}$ [mm]	6.1	5.7	6.6	8.6	8.1	5.8
b_2 [mm]	1.0	1.0	0	1.3	1.5	13.3
b_3 [mm]	4.4	4.1	6.8	5.8	5.5	5.2
η_s [–]	0.806	0.800	0.7	0.804	0.807	0.4
Input	Lv et al. [15]	RIT design code		Zhou et al. [35]	RIT design code	
q_m [kg/s]	1.80	1.80		12.74	12.74	
T_1 [°C]	669.9	669.9		400.0	400.0	
p_1 [bar]	106.9	106.9		193.1	193.1	
p_3 [bar]	77.7	77.7		76.3	76.3	
n, [krpm]	80.0	80.0		40.0	40.0	
Z [–]	21.0	21.0		12.0	12.0	
t_c, [mm]	0.3	0.3		-	0.10	
α_2, [deg]	76.5	76.5		73.0	73.0	
Output			Dev. [%]			Dev. [%]
R_2 [mm]	27.3	27.2	0.4	72.9	72.6	0.4
$R_{3,tip}$ [mm]	17.5	17.4	0.6	35.4	35.3	0.3
$R_{3,hub}$ [mm]	8.7	8.7	0.0	15.6	15.6	0.0
b_2 [mm]	4.5	4.3	4.4	3.1	3.2	3.1
b_3 [mm]	8.8	8.8	0.0	19.8	19.7	0.5
η_s [–]	0.831	0.872	4.7	0.854(1D) /0.825(CFD)	0.824	3.5 /0.1

$$F_{backdisk} = p_1 \frac{\pi}{4}\left(D_1^2 - D_{shaft}^2\right). \quad (11)$$

2.5. Impeller stress modeling

One of the key limiting factors in the design of turbomachinery is the impeller stress. In the preliminary design, a simple approach was preferred to give the first estimation of the maximum stress with the different turbine designs. This work utilizes the model presented by Osborne et al. [47] where the maximum disk stress is defined as a function of Poisson's ratio, impeller tip speed, and material density as:

$$\sigma_{max} = \frac{3+\nu}{8}\rho U_2^2. \quad (12)$$

The material used in this work is Ti-6Al-4 V, which is a commonly

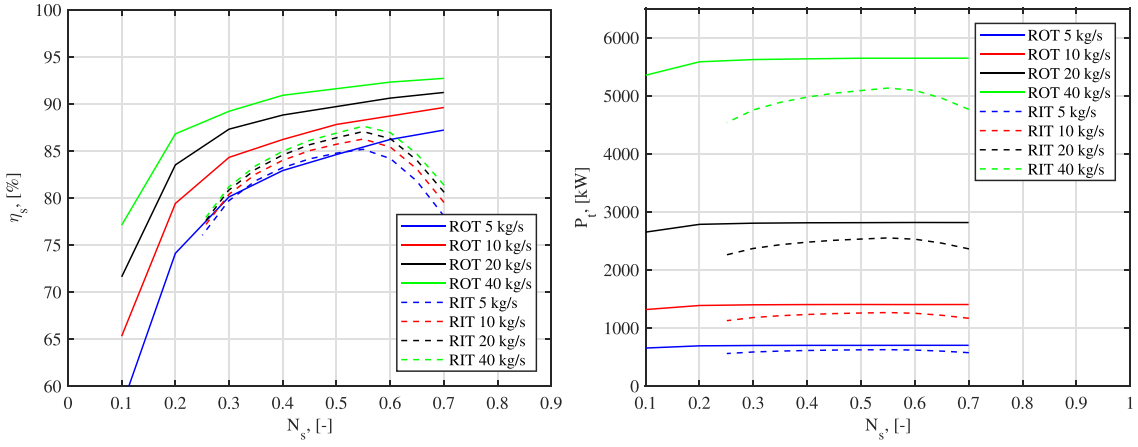

Fig. 3. Turbine isentropic efficiency (a) and fluid power (b) as a function of design specific speed.

used impeller material. Its density is 4430 kg/m^3, the yield stress at 600°C is 330 MPa according to Badea et al. [48], and a value of 0.342 is used for the Poisson's ratio.

3. Results

The main results of the study are presented in this section. The results for the turbine efficiency, geometry, rotational speed and loss distribution for the different designs are presented first. The main focus is on analyzing the results of ROT designs but in addition, the corresponding results for RIT designs are given as a comparison. Second, the results for the turbine axial force and strength analysis are presented.

3.1. Turbine efficiency, geometry and rotational speed

Both the turbine design mass flow and the specific speed significantly affect the performance of the ROT and RIT turbines, although the magnitudes are different. The results of turbine efficiencies with different design mass flow rates and with different design specific speeds are presented in Fig. 3a and the results of the turbine fluid power with the different designs are presented in Fig. 3b. The results are presented with tip clearance height of 0.3 mm for all the design cases. Based on the analysis, both the investigated turbine types were able to reach high efficiencies of well over 80%. In general, the higher the design mass flow rate of the turbine, the higher the predicted isentropic efficiency. With both turbine types, the higher efficiency with higher design mass flow rate mainly originated from the reduced tip clearance loss, due to the decrease in the relative clearance, when compared to a respective design with a lower design flow rate. In general, the RIT reached its maximum efficiency with design-specific speeds between 0.5–0.6 for all the studied design mass flow rates. The RIT efficiency is predicted to reduce notably, when designing the RIT for lower specific speeds than the optimal value. This is mainly caused by the increase in the stator losses at low specific speed designs [25,37]. The efficiency was predicted to drop even more steeply if the turbine is designed for a higher specific speed than its optimal value, mainly because of the increase in the exit kinetic loss. The ROT designs were predicted to reach relatively high efficiencies of over 80 % at wider range of design specific speeds, when compared to the RIT designs. The ROTs improved performance, especially in the low specific speed area, also supports its expected potential based on the previous understanding [20]. It is also worth mentioning that the design mass flow was predicted to have a more significant effect on the ROT performance compared to RIT designs. To examine the reasons behind the observed trends, the turbine loss distributions are discussed in more detail later in the next section.

The turbine geometry is affected by both the design conditions and by the turbine type. The effects of different design mass flow rates and specific speeds on ROT and RIT geometry are presented in Fig. 4a and in Fig. 4b. As the turbine design mass flow rate is increased, the blade height at the rotor inlet increases due to continuity equation. At the same time, the rotor outlet radius is increased. With ROTs this phenomenon is due to the need to increase the inlet radius so that a smooth blade height change can take place throughout the expansion. In addition, when designing the turbine with a low specific speed (= a low rotational speed), the turbine wheel becomes larger when compared to a high specific speed design. When comparing ROT and RIT designs with a comparable design mass flow rate and N_s, the rotor inlet blade height of the RIT is higher at low specific speed designs but the rotor inlet blade height becomes greater with ROT designs at higher specific speeds. With the investigated design cases the rotor inlet blade heights ranged between 3 mm to 12 mm with RIT designs and between 1 mm to 19 mm with the different ROT designs. The lowest blade heights of below 2 mm might lead to difficulties in the rotor wheel manufacturing as well as to increased tip clearance losses due to the high relative clearance with these designs. In general, the rotor dimensions are rather small in all the investigated cases with the rotor outer radii ranging from 0.02 m to 0.16 m with the RIT designs and from 0.02 m to over 0.4 m with the ROT designs. It should be also kept in mind, that the smallest values with ROTs may have potential risks of not allowing enough radial space to turn the flow smoothly from the axial to the radial direction. However, based on this work, the exact limit cannot be set since the result is case dependent and it is affected, for example, by the shaft and general flow

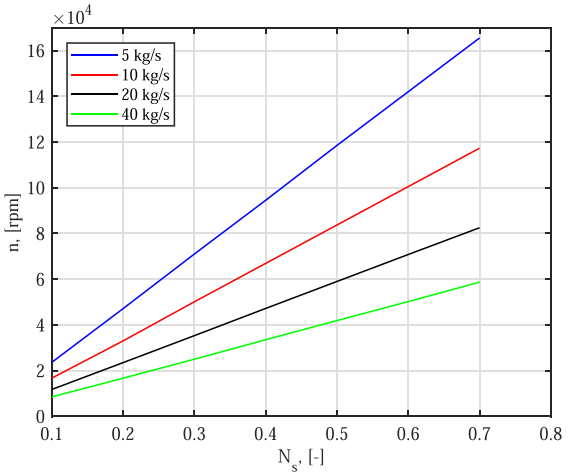

Fig. 5. Turbine rotational speed as a function of design specific speed. The results are comparable for both investigated turbine types.

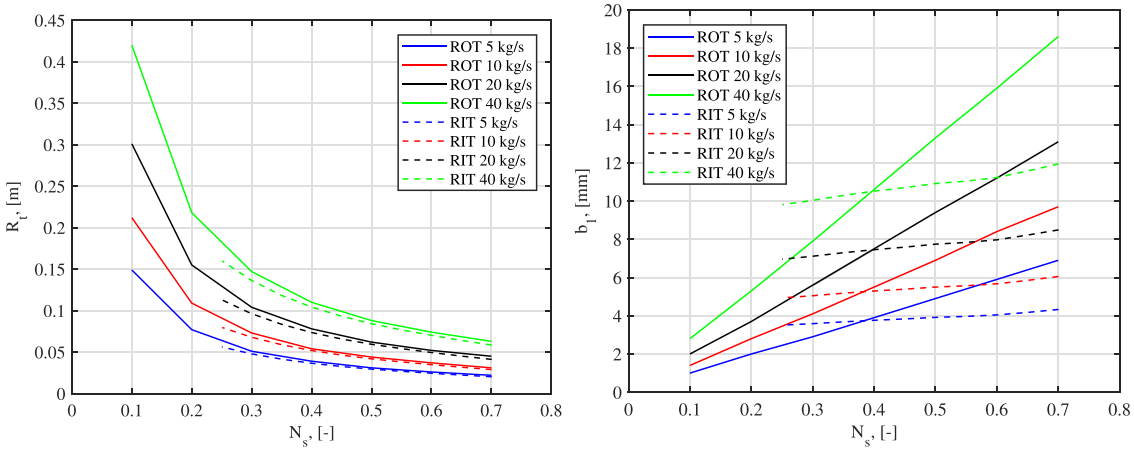

Fig. 4. Effect of the design specific speed on turbine outlet radius (a) and blade height at the turbine inlet (b).

layout designs.

The turbine rotational speed is one of the key limiting design parameters in supercritical carbon dioxide power systems. The rotational speed as a function of the turbine design specific speed is shown in Fig. 5. The results are applicable for both the investigated turbine types, as similar design conditions were considered for the both turbine types, resulting in similar rotational speeds with a comparable design specific speed. The higher the design power or the design specific speed, the higher also the requirement for the turbine rotational speed. The rotational speed is significantly increased with high N_s designs compared to the low N_s designs. In addition, the higher the design mass flow rate through the turbine, the lower the turbine rotational speed. The rotational speed of the 5 kg/s designs range from about 25 krpm to over 160 krpm, and with the highest mass flow rate of 40 kg/s from slightly below 10 krpm to about 60 krpm. Thus, the rotational speeds of the turbines can be considered to be significantly high, especially with the combination of the low mass flow rate and high specific speed design. The requirement for high rotational speed can make the rotordynamic design and generator design challenging when bearing in mind that the investigated power level of the machine is several hundreds of kW even with the lowest design mass flow. Exact rotational speed limits for the current high-speed electric machines cannot be determined, since they are always case dependent. To give an idea about what is currently achievable, Shen et al. [49] reported that Siemens has a high-speed permanent magnet electric machine with a nominal power of 5 MW and it rotates at 15,900 rpm, they also mentioned a 1 MW machine which rotates at 19,000 rpm. However, it should be stressed that these values are not definite limits but they give an impression of the current state. In future, much higher rotational speeds for MW-scale designs are also expected to become possible, e.g., with axially laminated anisotropic rotors [50]. Thus, especially the capability of ROTs to achieve high efficiencies at lower rotational speeds (low specific speeds) when compared to the RIT designs can be considered advantageous for the rotor dynamic design of the turbogenerator, as the rotational speeds tend to be significantly high, even with the high mass flow rate design. The use of more conventional step-down gearbox technology would also allow the rotational speed of the generator to be reduced and might allow higher rotational speeds for the turbines.

3.2. Turbine losses

The turbine loss distributions are given in the following for ROT designs and the results for the corresponding RIT designs are also presented for comparison. The losses are divided into stator losses, rotor losses, and tip clearance losses. The results are presented for designs with different mass flow rates and design specific speeds in Fig. 6a-c. The reason behind comparing these losses, instead of a more detailed loss component comparison, is that the loss generation of a radial outflow turbine differs from a radial inflow turbine in a fundamental level. The ROT behaves rather similarly to axial turbines, and the used loss correlation and the division of losses differ from RIT loss models. The tip-clearance loss is, however, a common loss source for both turbine types and a direct comparison is therefore justified.

In general, the turbine loss distributions differ considerably between the ROT and RIT designs. The stator loss decreases in the RIT design as the design specific speed is increased (6a). With the ROT design the stator loss is significantly higher with an $N_s = 0.1$ design when compared to the designs with higher N_s. The stator loss varies between 3 kJ/kg to 9

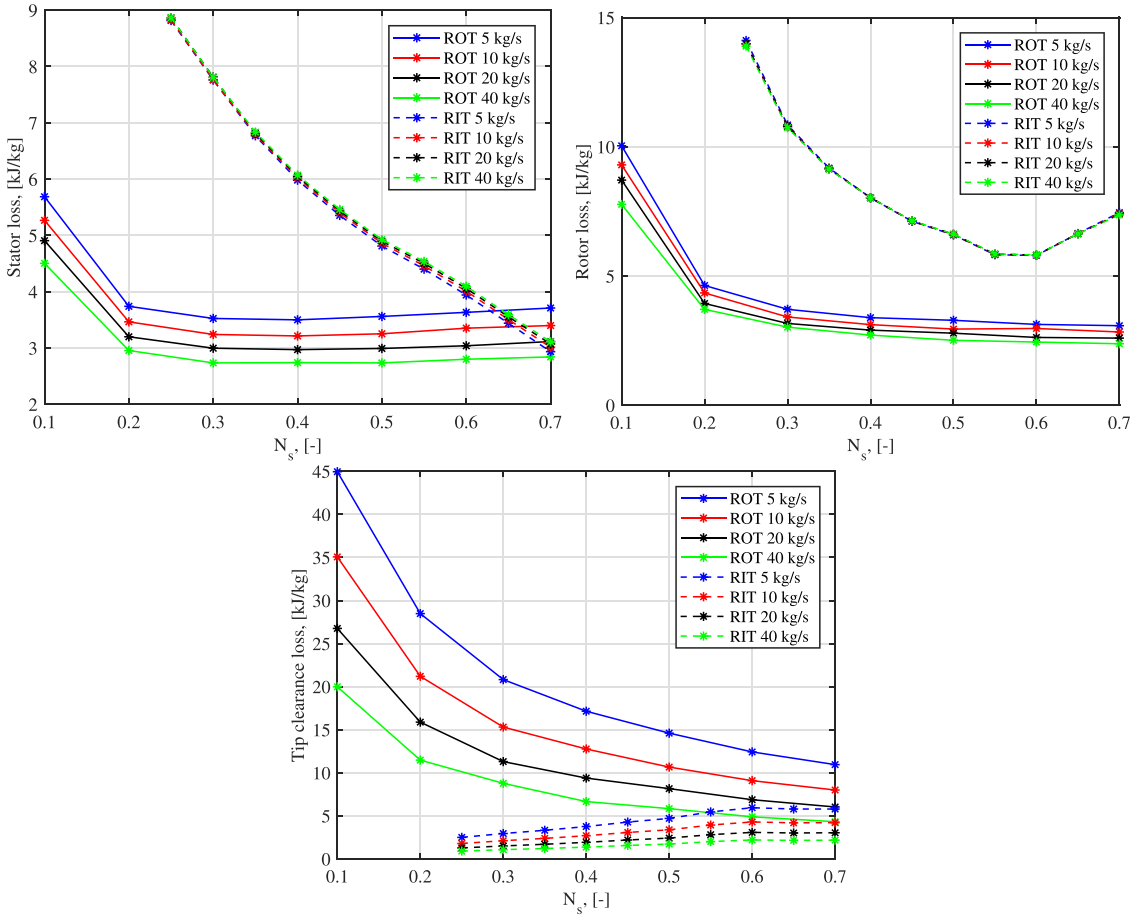

Fig. 6. Effect of design specific speed and design mass flow rate on predicted turbine losses: (a) presents the results for stator losses, (b) for rotor losses, and (c) for tip clearance losses.

kJ/kg with the RIT designs whereas slightly lower losses of below 3 kJ/kg to below 6 kJ/kg were predicted for the ROT. The losses predicted for the RIT remained nearly constant independently from the turbine power scale, despite the fact that the model takes into account the effect of the Reynolds number when defining the fiction factor. This is mainly because the nozzle solidity, stator inlet and outlet diameter ratios, as well as velocities were remained as nearly constant for the different designs. On the other hand, the stator loss model used for RITs does not take into account the effect of stator vane trailing edge blockage, which would increase the losses with the lowest design mass flow rates when compared to higher mass flow rates. More notable deviations in the stator loss between the different design mass flow rates were observed in the ROT designs. The reason behind the steep decrease in the ROTs stator loss is connected to the increase in the aspect ratio (b/c_r), which reduces the secondary losses. The aspect ratio increases towards higher specific speeds with ROTs but the stator Reynolds number reduces simultaneously, as shown in Table 4. This phenomenon compensates for the positive effects of higher aspect ratios and the stator losses remain nearly constant while the N_s increases. This phenomenon was not expected since usually the Reynolds number effects are associated with decreasing turbine sizes [38]. The Reynolds number effect also mainly explains the differences between different ROT designs when the mass flow (and turbine power) is changed in Fig. 6a.

The rotor loss was predicted to be lower in the ROT designs compared to the RIT designs. This can be explained by the larger rotor surface areas and higher curvature in RITs. For the RIT designs, the rotor losses were predicted to decrease when increasing the design N_s and the minimum rotor losses of below 6 kJ/kg were predicted with N_s between 0.5 to 0.6. At higher specific speeds the RIT rotor velocities start to increase, which leads to a notable increase in the rotor loss with high N_s designs. With ROTs the rotor loss is predicted to decrease when increasing the design N_s with loss values between 2 kJ/kg to 4 kJ/kg with the N_s between 0.2 to 0.7. The explanation behind the loss behavior with ROTs is similar to the stator, where the aspect ratio increases towards the higher specific speeds while the Reynolds number displays an opposite trend (see Table 4). There were also more deviations in the predicted losses with different mass flow rates for the ROT, whereas the variations in the RIT designs with different mass flows were predicted to be low. With ROTs, similarly to what was observed with the stator, the Reynolds number effects mostly explain the variation in losses due to the changing mass flow. The used passage loss model for RIT is mainly influenced by loss factor K_p, velocities, and flow angles, which remained nearly constant between the designs with different mass flow rates. Thus, the weakness of the used RIT passage loss model is that it does not directly take into account the Reynolds number effects, which would probably have some more notable influence on the rotor loss at different power scales. In general, the Reynolds numbers with the different RIT designs are in the same order of magnitude as in the corresponding ROT designs.

With both the turbine types, the tip clearance loss was predicted to increase as the turbine design mass flow decreases. This, can be explained by the fact that the relative clearance increases with lower mass flow rates, which leads to increased losses. Generally, higher tip clearance losses are predicted for ROT designs, where the lowest specific speeds experience clearly smaller blade heights than the RITs. In RIT designs the clearance loss was predicted to slightly increase as the design N_s was increased. This is mainly because the velocities at the rotor outlet increase with increasing N_s, influencing the clearance loss occurring near the rotor discharge. With ROT designs the tip clearance loss was predicted to decrease with the increase in the design N_s since the relative clearance is simultaneously reduced as well. It should be highlighted that the ROT tip clearance loss is influenced only by the axial clearance, whereas the RIT clearance loss is influenced by both the axial and radial clearances [51]. This fundamental difference can explain some of the observed differences in the magnitude of the tip clearance loss predictions, since it has been observed that for RITs the clearance loss is highly influenced by the flow through the radial clearance at the rotor exducer part [51].

3.3. Axial force and impeller stress analysis

The axial force analysis and a preliminary stress analysis for the different designs are presented in this section. The results of the axial force analysis are presented in Fig. 7a and the results of the impeller stress analysis are presented in Fig. 7b. The axial forces presented in Fig. 7a are presented as positive despite the direction of the force. In general, the force caused by the turbine impeller increases as the turbine design power is increased or as the design specific speed is decreased. This can be explained by the increased size of the impellers at high design power and with low specific speed designs. When comparing the two turbine types, the RIT designs have higher axial force, while with some of the ROT designs the back disk force is nearly compensated for by the outlet, shroud, and impulse forces. It is also important to remember, that the high axial force can reduce the shaft output notably as a significant amount of power is needed for compensating the axial force. In addition, the high axial force sets additional requirements for the design of the thrust bearings.

The results of the impeller stress analysis, presented in Fig. 7b are shown only for the 40 kg/s designs, as the different power levels resulted in impeller stresses at comparable level. This is because the peripheral velocities at the blade tip remain almost unchanged with the different design mass flow rates. The impeller stress was observed to be in the same order of magnitude for both turbine types in the range of 220 MPa to about 280 MPa. In general, the RIT designs lead to slightly lower stresses when compared to a ROT design with a comparable design N_s. The predicted stresses are at acceptable levels since they are below the 330 MPa yield stress at 600°C for the used Ti-Al6-4 V [48].

4. Conclusions

The design of supercritical CO_2 driven radial outflow turbines was analyzed and the designs were compared against respective radial inflow turbine designs. The two turbine types were designed with different CO_2 mass flow rates of 5 kg/s, 10 kg/s, 20 kg/s and 40 kg/s.

Table 4
Effect of design conditions on radial outflow turbine aspect ratio and Reynolds number. The results are presented for 40 kg/s and 5 kg/s cases, respectively.

Parameter	Mass flow	N_s=0.1	N_s=0.2	N_s=0.3	N_s=0.4	N_s=0.5	N_s=0.6	N_s=0.7
$b/c_{r,stat}$	40 kg/s	0.3	1.0	2.0	3.6	5.0	7.2	9.4
$b/c_{r,rot}$	40 kg/s	0.4	1.5	2.4	4.3	5.3	7.6	9.7
$b/c_{r,stat}$	5 kg/s	0.3	1.0	2.3	3.6	5.0	7.2	9.4
$b/c_{r,rot}$	5 kg/s	0.4	1.5	3.0	4.0	5.1	7.4	9.4
Re_{stat}	40 kg/s	3 204 000	2 869 000	2 422 000	1 936 000	1 736 000	1 478 000	1 323 000
Re_{rot}	40 kg/s	2 317 000	1 855 000	1 674 000	1 343 000	1 269 000	1 081 000	977 000
Re_{stat}	5 kg/s	1 133 000	1 017 000	791 000	675 000	582 000	496 000	438 000
Re_{rot}	5 kg/s	810 000	654 000	543 000	468 000	421 000	363 000	326 000

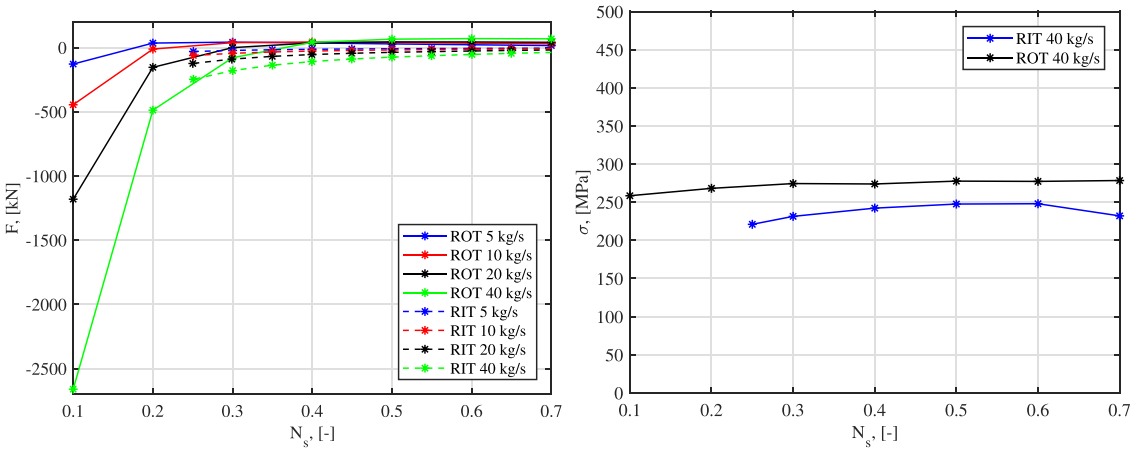

Fig. 7. (a) Axial force and (b) impeller stress.

The geometries and loss distributions for the different designs were analyzed and compared. The main conclusions of the study can be summarized as presented in the following:

- Radial outflow turbines can be designed for high efficiency at wider specific speed ranges compared to the investigated radial inflow turbines. Radial inflow turbines reach the peak efficiency at specific speed close to 0.5 to 0.6 and the efficiency is reduced steeply especially at higher design specific speeds.
- The required turbine rotational speeds are significantly high for both the studied turbine types, which could lead to challenges in electric machine design and rotor dynamics. One of the main benefits of using radial outflow turbines is their capability to achieve high turbine efficiencies at lower rotational speeds, compared to radial inflow turbines.
- For radial outflow turbines, the highest losses originate from the large relative tip clearance. Whereas, the use of a radial inflow turbine results in higher stator and rotor losses.
- The analysis of the axial force shows that the axial force is significantly high with ROT designs with the lowest specific speeds and highest design powers due to the large rotor diameters. This observation will set additional requirements for the shaft and thrust bearing design to compensate for the high axial force. However, by increasing the specific speed, the axial forces are almost compensated for with ROTs and are generally below the ones with RITs.
- In general, the rotor stresses were predicted to be at acceptable levels for both turbines when considering titanium wheels to be used.
- It can be concluded that the use of ROT instead of RIT increases the feasibility of the studied SCO2 systems without the need for a step down gear box if we consider the current rotational speed and blade height limits.

As a future work, it is suggested that more full-scale SCO_2 turbogenerator designs should be made in order to find exact limits with the current technology. On the other hand, it is also worth examining systems with advanced electric machines such as axially laminated anisotropic rotors. Also, experimental and CFD comparisons between radial outflow and radial inflow turbines should be performed for SCO_2 applications. In addition, it is important to develop more accurate turbine loss correlations and design guidelines for improved designs and loss estimations for different types of SCO_2 turbines. Especially, it is recommended that the effect of tip-clearance loss is studied more in detail in the future.

CRediT authorship contribution statement

Aki Grönman: Conceptualization, Methodology, Software, Validation, Formal analysis, Investigation, Writing – original draft, Writing – review & editing, Visualization. **Antti Uusitalo:** Conceptualization, Methodology, Software, Validation, Formal analysis, Investigation, Writing – original draft, Writing – review & editing, Visualization.

Declaration of Competing Interest

The authors declare that they have no known competing financial interests or personal relationships that could have appeared to influence the work reported in this paper.

Acknowledgements

Funding for the research work was received from LUT University and from Academy of Finland under the project “Loss mechanisms in expanding supercritical fluids” (Grant No. 323248). The funding for conducting the research work is greatly acknowledged by the authors.

References

[1] Li MJ, Zhu HH, Guo JQ, Wang K, Tao WQ. The development technology and applications of supercritical CO2 power cycle in nuclear energy, solar energy and other energy industries. Appl Therm Eng 2017;126:255–75.
[2] Dostal V, Hejzlar P, Driscoll MJ. High-Performance Supercritical Carbon Dioxide Cycle for Next-Generation Nuclear Reactors. Nucl Technol 2006;154(3):265–82.
[3] Kim YM, Sohn JL, Yoon ES. Supercritical CO2 Rankine cycles for waste heat recovery from gas turbine. Energy 2017;118:893–905.
[4] Uusitalo A, Ameli A, Turunen-Saaresti T. Thermodynamic and turbomachinery design analysis of supercritical Brayton cycles for exhaust gas heat recovery. Energy 2019;167:60–79.
[5] Iverson B, Conboy T, Pasch J, Kruizenga A. Supercritical CO2 Brayton Cycles for Solar-Thermal Energy. Appl Energy 2013;111:957–70.
[6] Yang J, Yang Z, Duan Y. Off-design performance of a supercritical CO2 Brayton cycle integrated with a solar power tower system. Energy 2020;117676.
[7] Ahn Y, Bae SJ, Kim M, Cho SK, Baik S, Lee JI, Cha JE. Review of supercritical CO2 power cycle technology and current status of research and development. Nucl Eng Technol 2015;47(6):647–61.
[8] Allam R, et al. Demonstration of the Allam Cycle: an update on the development status of a high efficiency supercritical carbon dioxide power process employing full carbon capture. Energy Proc 2017;114:5948–66.
[9] Kulhanek M, Dostal V. Supercritical carbon dioxide cycles thermodynamic analysis and comparison. In: Proc. SCCO2 Power Cycle Symp; 2011. p. 1–12.
[10] Sarkar J. Second law analysis of supercritical CO2 recompression Brayton cycle. Energy 2009;34(9):1172–8.
[11] Romei A, Gaetani P, Giostri A, Persico G. The role of turbomachinery performance in the optimization of supercritical carbon dioxide power systems. J Turbomach 2020;142(7).
[12] Li H, Zhang Y, Yao M, Yang Y, Han W, Bai W. Design assessment of a 5 MW fossil-fired supercritical CO2 power cycle pilot loop. Energy 2019;174:792–804.
[13] Wang, Y., Dostal, V., and Hejzlar, P. (2003). Turbine design for supercritical CO2 brayton cycle. In Global 2003, American Nuclear Society, pp. 1210–1220.
[14] Lee, J., Lee, J., I., Ahn, Y., and Yoon, H., (2012). Design methodology of supercritical CO2 brayton cycle turbomachineries. In Proceedings of ASME Turbo Expo 2012, no. GT2012-68933.

[15] Lv G, Yang J, Shao W, Wang X. Aerodynamic design optimization of radial-inflow turbine in supercritical CO2 cycles using a one-dimensional model. Energy Convers Manage 2018;165:827–39.
[16] Unglaube T, Chiang HWD. Preliminary Design of Small-Scale Supercritical CO2 Radial Inflow Turbines. J Eng Gas Turbines Power 2020;142(2).
[17] Lee S, Gurgenci H. A comparison of three methodological approaches for meanline design of supercritical CO2 radial inflow turbines. Energy Convers Manage 2020; 206:112500.
[18] Persky, R., Sauret, E., and Beath, A. (2015). Robust design and optimisation of a radial turbine within a supercritical co2 solar brayton cycle. In Proceedings of the 11th World Congress on Structural and Multidisciplinary Optimisation (WCSMO-11) (pp. 1–6). School of Aerospace, Mechanical and Mechatronic Engineering, University of Sydney.
[19] Fuller R, Preuss J, Noall J. Turbomachinery for supercritical CO2 power cycles. Proceedings of ASME Turbo Expo 2012;vol. 44717:961–6.
[20] Grönman A, et al. Design and verification of a hermetic high-speed turbogenerator concept for biomass and waste heat recovery applications. Energy Convers Manage 2020;225:113427.
[21] Pini M, Persico G, Casati E, Dossena V. Preliminary design of a centrifugal turbine for organic rankine cycle applications. J Eng Gas Turbines Power 2013;135(4).
[22] Casati E, Vitale S, Pini M, Persico G, Colonna P. Centrifugal turbines for mini-organic rankine cycle power systems. J Eng Gas Turbines Power 2014;136(12).
[23] Kim JS, Kim DY. Preliminary Design and Off-Design Analysis of a Radial Outflow Turbine for Organic Rankine Cycles. Energies 2020;13(8):2118.
[24] Luo D, Liu Y, Sun X, Huang D. The design and analysis of supercritical carbon dioxide centrifugal turbine. Appl Therm Eng 2017;127:527–35.
[25] Uusitalo A, Turunen-Saaresti T, Grönman A. Design and loss analysis of radial turbines for supercritical CO2 Brayton cycles. Energy 2021;120878.
[26] Balje OE. Turbomachines-a guide to design selection and theory. John Wiley; 1981.
[27] Rohlik Harold E. Analytical determination of radial inflow turbine design geometry for maximum efficiency. NASA 1968.
[28] Rohlik, H.E. Radial-Inflow Turbines. in Glassman, A.J. (Ed.). (1972). Turbine design and application (Vol. 290). Scientific and Technical Information Office, National Aeronautics and Space Administration.
[29] Ma, C., Qiu, Z., Gou, J., Wu, J., Zhao, Z., and Wang, W. (2018). Axial Force Balance of Supercritical CO2 Radial Inflow Turbine Impeller Through Backface Cavity Design. In Turbo Expo: Power for Land, Sea, and Air (Vol. 51180, p. V009T38A016). American Society of Mechanical Engineers.
[30] Whitfield A, Baines NC. a Design of radial turbomachines. Essex: Longman Scientific and Technical; 1990.
[31] Whitfield, A., and Wallace, F.J. (1973). a Study of incidence loss models in radial and mixed-flow turbomachinery, IME C55/73.
[32] Moustapha, H., Zelesky, M.F., Baines, N.C., and Japikse, D. (2003). Axial and radial turbines, Vol. 2 Concepts NREC Wilder.
[33] Jansen W. A Method for Calculating the Flow in a Centrifugal Impeller when Entropy Gradients are Present. Royal Society Conference on Internal Aerodynamics 1967 (Turbomachinery).
[34] Daily JW, Nece RE. Chamber dimension effects on induced flow and frictional resistance of enclosed rotating disks. Trans ASME J Basic Eng 1960;82:217–32.
[35] Zhou K, Wang J, Xia J, Guo Y, Zhao P, Dai Y. Design and performance analysis of a supercritical CO2 radial inflow turbine. Appl Therm Eng 2020;167:114757.
[36] Rahbar K, Mahmoud S, Al-Dadah RK, Moazami N. Modelling and optimization of organic Rankine cycle based on a small-scale radial inflow turbine. Energy Convers Manage 2015;91:186–98.
[37] Uusitalo A, Grönman A. Analysis of Radial Inflow Turbine Losses Operating with Supercritical Carbon Dioxide. Energies 2021;14(12):3561.
[38] Grönman, A., Uusitalo, A. and Turunen-Saaresti, T. (2020). Effects of design conditions and flow layout on the design of ultra-low aspect ratio radial outflow turbines. Proceedings of 14th European Conference on Turbomachinery Fluid Dynamics and Thermodynamics, April 12-16, 2021, Gdansk, Poland, ETC2021-548.
[39] Lemmon, E.W., Huber, M.L., McLinden, M.O. (2010). NIST standard reference database 23, reference fluid thermodynamic and transport properties (REFPROP), version 9.0. National Institute of Standards and Technology.
[40] Traupel W. Thermische Turbomaschinen. Berlin Heidelberg: Erster Band. Springer-Verlag; 1977.
[41] Persico G, Pini P, Dossena V, Gaetani P. Aerodynamic design and analysis of centrifugal turbine cascades. In: Proceedings of ASME turbo expo; 2013. GT2013-95770.
[42] Dixon SL. Fluid mechanics and thermodynamics of turbomachinery. fifth ed. Elsevier; 2005.
[43] Zhdanov, I., Staudacher, S. and Falaleev, S., (2013). An advanced usage of meanline loss systems for axial turbine design optimization. Proceedings of ASME Turbo Expo, Turbine Technical Conference and Exposition, June 3-7, San Antonio, Texas, USA. GT2013-94323.
[44] Qi J, Reddell T, Qin K, Hooman K, Jahn IH. Supercritical CO2 radial turbine design performance as a function of turbine size parameters. J Turbomach 2017;139(8): 081008.
[45] Nguyen-Schäfer H. Rotordynamics of Automotive Turbochargers. Switzerland: Springer International Publishing; 2015.
[46] Tiainen, J., Jaatinen-Värri, A., Grönman, A., Sallinen, P., Honkatukia, J. and Hartikainen, T. (2021). Validation of the Axial Thrust Estimation Method for Radial Turbomachines. International Journal of Rotating Machinery, 2021.
[47] Osborne C, Runstadler PW, Dodd Stacy W. Aerodynamic and mechanical design of an 8:1 pressure ratio centrifugal compressor. NASA CR-134782 1975.
[48] Badea L, Surand M, Ruau J, Viguier B. Creep behavior of Ti-6Al-4V from 450C to 600C. University Polytechnica Bucharest Scientific Bull Ser B 2014;76(1):185–96.
[49] Shen J, Qin X, Wang Y. High-Speed Permanent Magnet Electrical Machines – Applications, Key Issues and Challenges. CES Trans Electr Mach Syst 2018;2(1): 23–33.
[50] Abramenko V, Petrov I, Nerg J, Pyrhonen J. Synchronous reluctance motors with an axially laminated anisotropic rotor as an alternative in high-speed applications. IEEE Access 2020;8:29149–58.
[51] Dambach R., Hodson H.P, and Huntsman I. (1998). An experimental study of tip clearance flow in a radial inflow turbine. In Turbo Expo: Power for Land, Sea, and Air, vol. 78620, p. V001T01A110. American Society of Mechanical Engineers.